HHS Public Access

Author manuscript

Adv Healthc Mater. Author manuscript; available in PMC 2018 March 01.

Published in final edited form as:

Adv Healthc Mater. 2017 March ; 6(6): . doi:10.1002/adhm.201601080.

Chitosan-Gated Magnetic-Responsive Nanocarrier for Dual-modal Optical Imaging, Switchable Drug Release and Synergistic Therapy

Hui Wang, Dr.,
Department of Materials Science and Engineering, University of Washington, Seattle, Washington 98195 (United States)

Qingxin Mu, Dr.,
Department of Materials Science and Engineering, University of Washington, Seattle, Washington 98195 (United States)

Richard Revia, Dr.,
Department of Materials Science and Engineering, University of Washington, Seattle, Washington 98195 (United States)

Kui Wang, Dr.,
Department of Materials Science and Engineering, University of Washington, Seattle, Washington 98195 (United States)

Xuezhe Zhou,
Department of Materials Science and Engineering, University of Washington, Seattle, Washington 98195 (United States)

Peter J. Pauzauskie, Prof. Dr.,
Department of Materials Science and Engineering, University of Washington, Seattle, Washington 98195 (United States)

Fundamental & Computational Sciences Directorate, Pacific Northwest National Laboratory, Richland, WA 99354

Shuiqin Zhou, Prof. Dr., and
Department of Chemistry, The College of Staten Island, City University of New York, Staten Island, New York 10314 (United States)

Miqin Zhang, Prof. Dr.
Department of Materials Science and Engineering, University of Washington, Seattle, Washington 98195 (United States)

Abstract

Correspondence to: Miqin Zhang.

Supporting Information

Supporting Information is available from the Wiley Online Library or from the author.

The paper reports a dual-layer shell hollow nanostructure as drug carrier that provides instant on/off function for drug release and contrast enhancement for multi-modal imaging. The on-demand drug release is triggered by irradiation of an external magnetic field. The nanocarrier also demonstrates a high drug loading capacity and synergistic magnetic-thermal and chemo-therapy.

Graphical abstract

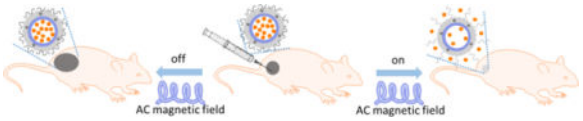

Keywords

drug carrier; chitosan valve; on/off release; multimodal imaging; synergistic therapy

Nanocarriers for drug delivery have been intensively studied owing to their ability to improve the therapeutic efficacy and minimize the adverse side effects of drugs in treating cancer and other diseases.[1] Despite the significant advances made in the past 10 years in the development of nanoparticles, the problems such as low drug loading capacity and inability to deliver an efficacious amount of chemotherapeutics to target cells limit their *in vivo* use to treat solid tumors.[2, 3] These limitations prompt the need to develop a multifunctional nanocarrier-based drug delivery system (DDS) that has high drug loading capacity, can provide a stimulus-triggered on/off drug release (also known as on-demand drug release), and has, desirably, a treatment monitoring capability.[4, 5] Mesoporous silica nanoparticles (MSNs) have been extensively investigated to serve as a DDS of high drug loading capacity due to their high pore volumes, large surface areas, and ease of surface functionalization for controlled drug release.[6–16] However, these MSNs lack the optical or magnetic properties needed for bioimaging and the ability of stimulus-triggered on/off drug release.[17–21] In addition, these MSNs easily agglomerate in aqueous solutions when loaded with drugs, and are potentially toxic to healthy tissues in the concentration range required for *in vivo* applications.[22]

To enable stimulus-triggered on/off drug release, materials including inorganic materials, polymers, and biomolecules have been studied to serve as capping or switching materials for nanocarriers with porous structures. These materials close the pores of the nanocarrier in default, and open the pores and release the drug in response to an endogenous or exogenous stimulus.[23–26] The stimulus can be a change in pH, temperature, enzyme concentration, redox potential, magnetic field, or light intensity.[27–35] Among these trigging mechanisms, exogenous activation of drug release has attracted considerable attention because it does not rely on changes in specific physical or chemical properties of the environmental medium.[36, 37] A promising drug release mechanism is through the engagement of an alternating current (AC) magnetic field, which turns on the drug release from a magnetic nanocarrier at a desired time after it reaches the site of action. Such a spatial-temporal control in drug administration may significantly improve the drug efficacy in cancer treatment.[38–43] However, despite burgeoning developments made in the past few years, it remains a challenge to produce stimulus-triggered on/off drug nanocarrier that has good

dispersity in aqueous solution, enables instant on/off drug release, and also serves as an imaging agent for non-invasive diagnosis and treatment monitoring.

In this study, we present a multifunctional yet structurally simple nanocarrier that has a high drug loading capacity, releases drug in response to onset of an AC magnetic field, and can serve as a long-term imaging contrast agent and effectively kills cancer cells by synergistic action. This nanocarrier (HMMC-NC) has a spherical shell structure with a center cavity of 80 nm in diameter. The shell is comprised of two layers: an inner layer of magnetite that exhibits superparamagnetism and an outer layer of mesoporous carbon embedded with carbon dots that exhibit photoluminescence property. Thus in addition to being a drug carrier, HMMC-NC is also a contrast agent for bioimaging. The switchable drug release is enabled by the chitosan molecules attached on the nanocarrier as the switching material which turns on or off the drug release in response to the application or withdrawal of an AC magnetic field.

Figure 1 shows the schematic diagram for the production of the magnetic-responsive drug delivery system and its switchable drug release process trigged by an AC magnetic field. A dual-layer shell is coated on a SiO_2 nanoparticle (NP) at 200°C using ferrocene as precursor (Figure 1a). The ferrocene quickly decomposes at the high temperature to form positively-charged iron and negatively-charged cyclopentadiene.[44] The resultant positively-charged iron atoms are adsorbed onto the surface of the negatively-charged SiO_2 NP by electrostatic attraction.[45] The positively-charged SiO_2@iron hybrid NP is then again surrounded by negatively-charged cyclopentadiene by the electrostatic attraction between the SiO_2@iron hybrid NP and cyclopentadiene. Finally, O_2 resulting from decomposition of H_2O_2 oxidizes the iron to form magnetite and oxidizes cyclopentadiene to form disordered (amorphous carbon) or ordered (carbon dot) carbon structures under the high temperature and high pressure from the gasification of the solvent acetone, leading to the formation of the SiO_2@Fe_3O_4@carbon core-shell-shell NP. The SiO_2 core is removed through erosion by soaking the resultant sample in ammonia water at high temperature and pressure, which leads to the formation of a nanostructured shell (i.e., HMMC-NCs, Figure 1b). Doxorubicin (DOX), a common anti-cancer drug, was used here as a model drug to examine the drug loading capacity of HMMC-NCs. The drug loading is achieved by soaking HMMC-NCs in a phosphate buffered saline (PBS) solution of DOX (Figure 1c). DOX-loaded HMMC-NCs are then further surface-modified with chitosan molecules which act as valves to seal the DOX when no AC magnetic field is present (Figure 1d).

The morphology and structure of as-prepared HMMC-NCs were characterized by transmission electron microscopy (TEM). As shown in Figure 2a–c, all SiO_2 template NPs, SiO_2@Fe_3O_4@carbon NPs, and Fe_3O_4@carbon NPs have a uniform size distribution (with diameters of 78 nm, 120 nm and 122 nm, respectively) and a spherical shape. The core-shell-shell structure of SiO_2@Fe_3O_4@carbon NPs is confirmed by high-angle annular dark-field scanning transmission electron microscopy (HAADF-STEM) (Figure S1, Supporting Information). Energy dispersive X-ray (EDX) elemental mapping in single SiO_2@Fe_3O_4@carbon NP reveals that elements Si, Fe and C are mainly distributed in the core, inner shell and outer shell, respectively. Notably, the TEM image in Figure 2c reveals the hollow nanostructure of Fe_3O_4@carbon NPs. The high-resolution TEM image in Figure

2d shows a dual-layer shell structure from a single Fe_3O_4@carbon NP and reveals that the inner layer with darker contrast is composed of magnetite nanocrystals and the outside layer with lighter contrast is composed of carbon. Nanocrystals with a size of ~3 nm can be observed in the carbon shell (marked with a dashed circle in Figure 2d). The EDX spectrum (Figure S2a, Supporting Information) of a single nanocrystal embedded in the carbon shell reveals the presence of only C and Cu elements, indicating that the nanocrystals are carbon dots. The 2D lattice fringes (Figure S2b, Supporting Information) of the carbon dots demonstrate an interplanar distance of about 0.204 nm, which corresponds to the (102) lattice planes of graphitic (sp^2) carbon.[46] The crystallographic structure and phase purity of the as-prepared nanocarrier were examined by X-ray powder diffraction (XRD) and Raman scattering techniques. Cu is from the TEM grid. The observed reflections of 220, 311, 400, 422, 511 and 440 in the XRD pattern (Figure 2e) can be indexed to the magnetite's crystal structure (Fe_3O_4).[47] The Raman scattering pattern (Figure 2f) of the nanocarrier contains peaks at 1575 cm^{-1} and 1348 cm^{-1}, which correspond to the G mode and D mode of the carbon material, respectively.[48, 49] These results indicate that the nanocarrier is composed of magnetite and carbon materials.

The resultant chitosan-HMMC-NCs showed no discernable changes in morphology (Figure 2g) as compared to HMMC-NCs (Figure 2c). Figure S3 (Supporting Information) shows the UV–Vis absorption spectra of chitosan, HMMC-NCs and chitosan-HMMC-NCs. While chitosan has no significant absorption at wavelengths above 200 nm, HMMC-NCs exhibits a broad peak centered at 254 nm, which corresponds to the π-π^* transition of aromatic domains in the carbon shell.[50] The chitosan-HMMC-NCs show a similar absorption peak centered at 254 nm, indicating that the surface modification did not change the optical properties of HMMC-NCs. A comparison of FT-IR spectra (Figure S4, Supporting Information) of chitosan, HMMC-NCs and chitosan-HMMC-NCs was made to confirm the successful surface modification of chitosan on HMMC-NCs. The amide II and amide I bands in free chitosan are present in the spectrum of chitosan-HMMC-NCs, but the bands shift from 1521 cm^{-1} to 1528 cm^{-1} for amide I and from 1660 cm^{-1} to 1675 cm^{-1} for amide II. Similarly, the characteristic absorption peaks of the –OH and –COOH groups on the surface of HMMC-NCs are present in the spectrum of chitosan-HMMC-NCs, but the corresponding bands shift from 3400 cm^{-1} to 3570 cm^{-1} for –OH groups and from 1702 cm^{-1} to 1727 cm^{-1} for –COOH groups. These peak shifts indicate that chitosan molecules have been successfully immobilized on HMMC-NCs through amidation reaction and hydrogen bonding between HMMC-NCs and chitosan molecules. In addition, the hydrogen bonding interaction between HMMC-NCs and chitosan molecules could be confirmed by the –OH stretching vibration shift in both HMMC-NCs and chitosan molecules. The above results indicate that HMMC-NCs and chitosan have stable chemical bonding interactions in chitosan-HMMC-NCs.

Zeta potential measurements (Figure 2h) further indicate the successful surface modification of HMMC-NCs with chitosan. HMMC-NCs have a negative zeta potential (–29.2 ± 0.6 mV) and chitosan-HMMC-NCs have a positive zeta potential of 14.8 ± 0.8 mV. Chitosan has a positive zeta potential of 19.1 ± 0.9 mV. The hydrodynamic diameter (D_h) distributions of HMMC-NCs and chitosan-HMMC-NCs in water are shown in Figure S5a (Supporting Information). Compared to HMMC-NCs, the larger diameter of chitosan-HMMC-NCs was

likely due to a result of the presence of positively-charged chitosan adsorbed onto the surface of the negatively-charged carbon shell of HMMC-NCs. Chitosan-HMMC-NCs dispersed in PBS demonstrated excellent stability in 7 days (Figure S5b, Supporting Information). Full nitrogen adsorption isotherms (Figure 2i) were acquired to obtain the information about the specific surface areas and pore sizes of HMMC-NCs and chitosan-HMMC-NCs. The Brunauer–Emmett–Teller (BET) surface area and total pore volume of HMMC-NCs were 240.23 $m^2 g^{-1}$ and 0.689 $cm^3 g^{-1}$, respectively, which are greater than those of chitosan-HMMC-NCs (14.57 $m^2 g^{-1}$ and 0.09 $cm^3 g^{-1}$). In addition, HMMC-NCs and chitosan-HMMC-NCs demonstrate a similar pore size distribution from 2 nm and 6 nm (Figure S6, Supporting Information). These results indicate that chitosan-HMMC-NCs not only show an appreciable absence of mesoporosity but also have significant pore blocking due to the presence of chitosan molecules as valves.

To assess the optical properties of chitosan-HMMC-NCs, a detailed photoluminescence (PL) study was performed at different excitation wavelengths (l_{ex}). As shown in Figure S7a (Supporting Information), when l_{ex} increases from 260 nm to 520 nm, the emission peak gradually shifts to longer wavelengths and the PL intensity gradually increases and then decreases. Notably, the PL spectra (Figure S7b, Supporting Information) of chitosan-HMMC-NCs excited by long-wavelength light from 1000 nm to 700 nm demonstrate upconverted emissions from 550 nm to 454 nm. The upconversion PL behavior of chitosan-HMMC-NCs can be attributed to multiphoton active processes of the carbon dots embedded in the carbon shell.[51]

SF-763 human glioblastoma cells were selected as a model to evaluate the ability of chitosan-HMMC-NCs to serve as a fluorescent marker for cellular optical imaging. Figure 3a–c show fluorescence confocal images of SF-763 cells that had been incubated with chitosan-HMMC-NCs for 2 h under laser irradiation at wavelengths of 405 nm, 488 nm and 546 nm, respectively. Clearly, chitosan-HMMC-NCs produced a bright fluorescence and illuminated SF-763 cells in multicolor forms. As shown in Figure S8 (Supporting Information), the confocal images of SF-763 cells do not show a fluorescent signal change after continuous irradiation with an excitation laser at 405 nm for 60 days, indicating the excellent stability of chitosan-HMMC-NCs as optical maker. Since these fluorescent carbon dots are embedded in the mesoporous carbon outer shell, chitosan-HMMC-NCs can be used for long-term cellular imaging.

Due to low photobleaching, weak auto-fluorescence, and deep penetration in biological tissues, two-photon fluorescence microscopy has attracted much attention since its invention by Webb et al., in 1990.[52, 53] As shown in Figure S6b (Supporting Information), chitosan-HMMC-NCs exhibit upconverted PL properties. Thus, we assessed the possibility of two-photon fluorescence imaging of cells treated with chitosan-HMMC-NCs. Figure 3d–f shows images of diamidino-2-phenylindole (DAPI) stained nuclei (d), two-photon fluorescence (e), and their overlay (f) of SF-763 cells after they were treated with chitosan-HMMC-NCs and excited by a femtosecond infrared laser of 900 nm. It is clear that the treated cells can be illuminated by the upconverted fluorescence emitted by chitosan-HMMC-NCs under excitation of an NIR laser. These imaging results confirm that chitosan-HMMC-NCs can penetrate cell membrane, enter and light up tumor cells in multicolor form. Furthermore, in

vivo NIR imaging with chitosan-HMMC-NCs was investigated by injecting them into the tumors of nude mice. As shown in Figure S9 (Supporting Information), the fluorescence signal of chitosan-HMMC-NCs is observed at excitation wavelengths of 605 and 640 nm using an IVIS imaging system.

To characterize the magnetic property of chitosan-HMMC-NCs, samples were examined using a superconducting quantum interference device magnetometer. As shown in Figure 3g, chitosan-HMMC-NCs demonstrate superparamagnetic behavior at 300 K since no hysteresis loop is found. The saturation magnetization (Ms) of chitosan-HMMC-NCs is found to be 23.45 emu/g. Figure 3h shows the rapid temperature increase for HMMC-NCs and chitosan-HMMC-NCs under an AC magnetic field while there is no temperature increase in water (control) irradiated by the same source, demonstrating the effective magnetic-thermal conversion by these nanocarriers. The IR thermal imaging of chitosan-HMMC-NCs under different irradiation time (0 min and 30 min) shows the increased temperature from 23.6°C to 28.9°C and further verifies their magnetic-thermal conversion property (Figure 3i). MRI contrast enhancement ability of chitosan-HMMC-NCs at different concentrations was assessed. An R_2 map (Figure 3j) shows that the MRI signal intensity reduces with an increase in iron concentration. A linear correlation of R_2 relaxation with iron concentration is established (Figure S10, Supporting Information). The R_2 relaxivity of chitosan-HMMC-NCs is found to be 75.5 s^{-1} mM^{-1} at 14 T. The in vivo MRI of chitosan-HMMC-NCs (100 μL, 0.5 mg/mL) was further assessed by subcutaneous injection. chitosan-HMMC-NCs demonstrated an apparent contrast enhancement in the NC-injected site as compared to PBS-injected area (Figure S11, Supporting Information).

DOX molecules can be readily loaded into HMMC-NCs, and drug loading was assessed by measuring the absorbance of DOX using a UV-vis spectrometer. The appearance of the characteristic UV-Vis absorption peak of DOX around 480 nm confirms the successful loading of the chemotherapeutic into chitosan-HMMC-NCs (Figure S12, Supporting Information). The drug loading capacity of HMMC-NCs for DOX reaches as high as 53.07 wt%. The high drug loading capacity of HMMC-NCs is attributed to the unique structure of the NCs, namely large central cavity and numerous mesopores in the magnetite@carbon dual-layer shell, combined with the contribution of interactions between DOX molecules and HMMC-NCs including supramolecular p-stacking, hydrogen bonding and electrostatic attractions.[54–56] To achieve the external stimulus-triggered on/off release of DOX from HMMC-NCs, DOX-loaded HMMC-NCs were surface-modified with chitosan molecules serving as on/off valves. The chitosan molecules interact both covalently (amidation) and electrostatically with the negatively-charged molecules of underlying mesoporous carbon layer and thus, serve as capping material that blocks the outflow of the preloaded drug in the material's pores. The drug loading capacity of chitosan-HMMC-NCs was slightly reduced to 48.21 wt%, due to the release of DOX from HMMC-NCs during the surface modification process as compared to HMMC-NCs (53.07 wt%).

To assess the function of chitosan as drug release valves, the *in vitro* release of DOX from both DOX-loaded HMMC-NCs (i.e., no chitosan capping for comparison) and DOX-loaded chitosan-HMMC-NCs was investigated using a dialysis membrane against PBS solution. Figure 4a compares the DOX release profiles of HMMC-NCs dispersed in PBS solution at

37°C, without/with AC magnetic field irradiation for 30 mins at different time points of 0, 8, 26 and 50 h after the nanocarriers were dispersed into the PBS solution. Without magnetic field irradiation, the release of DOX from HMMC-NCs is relatively slow and at a nearly constant rate after first 12 h; 27.5% of the loaded DOX was released from HMMC-NCs in 78 h. In contrast, under the magnetic field irradiation, the release of DOX from HMMC-NCs substantially speeded up. When the magnetic field was removed, the drug release returned to its regular, slower rate. About 47.6% of loaded DOX was released from HMMC-NCs in 78 h under AC magnetic field irradiation. Figure 4b shows the DOX releasing behaviors of chitosan-HMMC-NCs dispersed in PBS solution at 37°C, with/without AC magnetic field irradiation. Without AC magnetic field irradiation, only 4.2% of loaded DOX was released from chitosan-HMMC-NCs in 78 h, indicating that the chitosan valves effectively prevented the drug release from chitosan-HMMC-NCs. Comparing to the result for HMMC-NCs (without chitosan as drug release valves) shown in Figure 4a, a much greater DOX release rate was observed for HMMC-NCs when no magnetic field was applied. Figure 4b also shows the drug release profile of chitosan-HMMC-NCs when they were subjected periodically to the irradiation of a magnetic field. Here, at the beginning of each 10-hour cycle, chitosan-HMMC-NCs were irradiated by the magnetic field for 30 min, and then the irradiation was turned off for 9.5 h. The accumulated drug release from chitosan-HMMC-NCs was recorded for a period of 80 hrs. As shown, for each 10-hour cycle, at onset of the magnetic irradiation, the DOX release from chitosan-HMMC-NCs surged and then remained at a high release rate during 30-min irradiation. During the 9.5-hour period when the irradiation was turned off, minimal drug release was observed. These results indicate that chitosan molecules in chitosan-HMMC-NS can effectively serve as valves to instantly turn on/off the drug release, controllable by an external AC magnetic field.

This magnetic-triggered drug release is produced by heating of the drug carrier through magnetic-thermal conversion. The heat produced under AC magnetic field weakens the drug-host interactions between DOX and the carboxyl group of HMMC-NCs, and also increases the mobility of DOX at an elevated temperature. More importantly, because chitosan is positively-charged while HMMC-NCs is negatively charged, the chitosan molecules can adsorb on the surface of the carbon shell via electrostatic interactions, resulting in the “off” state for DOX release from DOX-loaded chitosan-HMMC-NCs. When the magnetic field is applied, leading to an increase in local temperature, the weak electrostatic and hydrogen bonding interactions between the carbon shells and chitosan molecules are disrupted, leading to the “on” state for DOX release. When the magnetic irradiation is removed, the chitosan molecules can return to their original interactive state (electrostatic and hydrogen bonding interactions) with HMMC-NCs, closing the pores again and shutting off the drug release.

We further investigated the *in vitro* chemo therapy, magnetic-thermal therapy and combined therapy of SF-763 cells with HMMC-NCs and chitosan-HMMC-NCs. Figure 4c shows the *in vitro* cytotoxicity of drug-free and DOX-loaded HMMC-NCs without and with an AC magnetic field irradiation for 30 min. Drug-free HMMC-NCs showed negligible cytotoxicity against SF-763 cells after 72 h incubation without magnetic irradiation for concentrations up to 50 μg/mL. In contrast, the cell viability dramatically decreased when the cells were treated with DOX-loaded HMMC-NCs under the same conditions due to the therapeutic

effect of DOX molecules released from HMMC-NCs. Furthermore, SF-763 cells were irradiated with an AC magnetic field for 30 min during the incubation process with drug-free HMMC-NCs and DOX-loaded HMMC-NCs. The cytotoxicity results show that the 30-min magnetic field irradiation increased the cell kill by drug-free HMMC-NCs suggesting that HMMC-NCs can serve as an effective magnetic-thermal therapy agent. Further, in a control experiment, 30-min of magnetic field irradiation alone (no nanocarriers involved) showed little influence on the cytotoxicity (Figure S13, Supporting Information), further suggesting that it was the magnetic-thermal effect of HMMC-NCs, rather than the irradiation itself, contributed to the cell killing. Notably, the combined treatment of 30-min AC magnetic field irradiation and DOX released from DOX-loaded HMMC-NCs (HMMC-NCs+DOX +magnetic field) kills tumor cells even more effectively than the treatment with either DOX-loaded HMMC-NCs (HMMC-NCs+DOX, chemotherapy) or 30 min AC magnetic field irradiation therapy (HMMC-NCs+magnetic field, magnetic-thermal therapy) alone.

Figure 4d shows the *in vitro* cytotoxicities of drug-free and DOX-loaded chitosan-HMMC-NCs without and with AC magnetic field irradiation for 30 min. More than 91% of the SF-763 cells survived after 72 h treatment with drug-free chitosan-HMMC-NCs at concentrations up to 50 μg/mL without magnetic field irradiation. Meanwhile, more than 88% of SF-763 cells and HEK293T cells survived after 72 h treatment with chitosan-HMMC-NCs at a higher concentration up to 1000 μg/mL (Figure S14, Supporting Information). Interestingly, without magnetic field irradiation, DOX-loaded chitosan-HMMC-NCs also demonstrate negligible cytotoxicity against SF-763 cells after 72 h incubation for the same concentration range. These results indicate that chitosan valves can effectively prevent DOX release from chitosan-HMMC-NCs. In order to observe the treatment efficacy of the magnetic-triggered drug release, SF-763 cells were treated with chitosan-HMMC-NCs and DOX-loaded chitosan-HMMC-NCs, and irradiated with a magnetic field for 30 min during the incubation process. The results show that drug-free chitosan-HMMC-NCs effectively killed tumor cells with the assistance of 30 min magnetic field irradiation and had a similar cell-killing efficiency as HMMC-NCs also under 30 min magnetic field irradiation.

It is expected that the combination of magnetic-thermal effect with magnetic–triggered drug release from HMMC-NCs or chitosan-HMMC-NCs will provide synergistic effects for cancer therapy. Figure 4e and f shows a comparison of the therapeutic efficacies of HMMC-NCs and chitosan-HMMC-NCs as DOX carriers and magnetic-thermal therapy agents (calculated by subtracting the cell viability from 100%) for independent chemotherapy and magnetic-thermal treatments, as well as the combined chemo/magnetic-thermal therapy. Also included in the efficacy analysis is an additive efficacy estimated as $T_{additive} = 100 - (f_{chemo} \times f_{magneticthermal}) \times 100$, which represents the therapeutic efficiency of a simple combination of chemotherapy and magnetic-thermal therapy, where f_{chemo} and $f_{magneticthermal}$ are the fraction of surviving cells after independent chemotherapy and magnetic-thermal therapy, respectively.[57] The therapeutic efficacies of the combined chemo-magnetic-thermal therapy for both HMMC-NCs and chitosan-HMMC-NCs were significantly higher than the additive therapeutic efficacy of chemo- and magnetic-thermal therapy, indicating the synergistic effect plays significant role in the overall therapeutic efficacy. When a t-test is used to compare the efficacy of the combined chemo-magnetic-

thermal treatment to the additive efficiencies of independent chemo and magnetic-thermal treatments, all p-values are smaller than 0.01, indicating a significant difference. This suggests that these NCs may allow physicians to use lower dosages of chemotherapeutics to treat cancer patients to reduce the systemic side effects. The ratio of the combined treatment efficacy to the additive treatment efficacy at the same concentration was used to evaluate the synergistic effect of various NCs. Result shows that the ratio for DOX-loaded chitosan-HMMC-NCs at three concentrations (average = 2.17) is greater than the ratio for DOX-loaded HMMC-NCs at the same three concentrations (average = 1.55). This indicates that the surface modification of DOX-loaded HMMC-NCs with chitosan further improves the therapeutic efficacy of these NCs.

In vivo toxicity of nanostructured materials is a major concern in biomedical applications. To assess the toxicitity of chitosan-HMMC-NCs and DOX-loaded chitosan-HMMC-NCs *in vivo*, they were injected into wild-type mice via tail veins. The mice were sacrificed 5 days post-injection, organs (heart, kidney, liver, lung and spleen) were harvested, fixed, stained, and histologically analyzed. As shown in Figure 5a, no discernible toxicity sign was observed in mice treated with chitosan-HMMC-NCs or DOX-loaded chitosan-HMMC-NCs as compared to control mice receiving no treatment, suggesting that DOX was well encapsuled in chitosan-HMMC-NCs.

The biodistribution of chitosan-HMMC-NCs were investigated by injecting them into wide-type mice via tail veins. Mice were sacrificed at 24, 48, and 72 h post-injection, whole organs (liver, spleen, kidney, lung, and heart) were removed from mice, and the fluoresnce intensity of each organ was assessed by an IVIS imaging system. As expected, liver was the dominant organ in maintaining chitosan-HMMC-NCs accumulation as a result of reticuloendothelial system (RES) uptake, followed by kidney, stomach, spleen, lung and heart. After 96 h post-injection, very small amounts of chitosan-HMMC-NCs remianed in liver, kidney and spleen, and nearly no chitosan-HMMC-NCs were found in lung and heart.

To evaluate the on-demand drug release capability and therapeutic efficacy of chitosan-HMMC-NCs in vivo, mice bearing C6 tumors were administrated with the nanocarriers by intratumoral injection. C6 cells were chosen because they grow fast to generate invasive tumors that are difficult to treat. Mice bearing C6 tumors were randomly divided into 4 groups with five mice per group that were treated with PBS plus AC magnetic field, chitosan-HMMC-NCs plus AC magnetic field, DOX-loaded chitosan-HMMC-NCs with or without AC magnetic field, respectively. The nanocarriers were injected into mice every 3 days for a total of four times. Tumor volumes were measured every other day for two weeks after the intratumoral injection. As shown in Figure 5c and d, mice injected with PBS solution and treated with AC magnetic field demonstrated the greatest tumor growth. Tumors in mice treated with DOX-loaded chitosan-HMMC-NCs but not AC magnetic field showed only slightly reduced growth likely due to the slow release of DOX as compared with mice treated PBS solution. A similar tumor growth rate was observed in mice treated with chitosan-HMMC-NCs and AC magnetic field. Notably, the treatment with DOX-loaded chitosan-HMMC-NCs and AC magnetic field resulted in marked inhibition of tumor growth. After four rounds of this treatment, the tumors exhibited no further growth. In addition, mice did not show apparent body weight loss after the treatment.

At day 14, tumors from all mouse groups were harvested and weighed (Figure 5e). Compared to the treatment with chitosan-HMMC-NCs and AC magnetic field (magnetic-thermal therapy) or with DOX-loaded chitosan-HMMC-NCs without AC magnetic field (chemo-therapy), the therapeutic efficacy achieved by the combinatory therapy (DOX-loaded chitosan-HMMC-NCs with AC magnetic field) appeared to be much higher than the additive efficacy of magnetic-thermal and chemo-therapy alone based on the tumor growth reduction ratio at the day 14, suggesting an synergistic effect by the combinatory therapy.[58] Hematoxylin and eosin (H&E) staining of tumor sections (Figure 5f) further confirmed that tumors in control groups retained their normal morphology with distinctive membrane and nuclear structures, whereas most tumor cells in mice receiving DOX-loaded chitosan-HMMC-NCs with AC magnetic field were severely damaged with disappeared nuclei.

In summary, we have developed a simple, effective, and multifunctional magnetic-triggered drug delivery system with controllable instant on/off release behavior. The resultant chitosan-HMMC-NCs not only demonstrate magnetic-thermal conversion property, but also serve as confocal and two-photon imaging contrast agents. Chitosan-HMMC-NCs demonstrate a high loading capacity (48.21 wt%) for anti-cancer drug DOX. The presence of positively-charged chitosan on the carbon shell of HMMC-NCs allows to instantly turn on or off the drug release in response to the application of an AC magnetic field irradiation that heats up the superparamagnetic magnetite nanocrystals in the inner layer of HMMC-NCs. In addition to the magnetic-trigger drug release, the magnetite nanocrystals also generate magnetic-thermal effect to kill tumor cells. More significantly, DOX-loaded chitosan-HMMC-NCs demonstrate a synergistic effect for cancer therapy.

Experimental Section

Materials

Doxorubicin (DOX) was purchased from LC Laboratories (Woburn, MA). All other chemicals were purchased from Sigma-Aldrich (St. Louis, MO). Ferrocene ($Fe(C_5H_5)_2$, ≥ 98%), hydrogen peroxide (H_2O_2, 30%), acetone (C_3H_6O, 99%), ethanol (C_2H_6O, 99%), tetraethyl silicate (TEOS, 98%), ammonia water ($NH_3{\cdot}H_2O$, 27%), chitosan (low molecular weight), and 1-ethyl-3-(3-dimethylaminopropyl) carbodiimide hydrochloride (EDC) were used as received.

Synthesis of SiO_2 NPs

Monodispersed SiO_2 NPs were synthesized following the Stöber method. Briefly, 75 mL ethanol and 6 mL ammonia water were mixed in a conical flask (125 mL). The resultant solution was vigorously stirred for 20 min at 45 °C. 1.0 mL TEOS was quickly added, and the mixture solution was vigorously stirred for 2 h. The resultant SiO_2 NPs were purified with repeated centrifugation (12,000 rpm, 10 min) and redispersion in water for five cycles. Finally, the aqueous dispersion of SiO_2 NPs with a concentration of 4 mg/mL was collected for further use.

Synthesis of SiO_2@Fe_3O_4@carbon NPs

0.10 g ferrocene and 0.5 mL SiO_2 NP solution (4 mg/mL) were dispersed in 30 mL acetone. After the solution was intensely sonicated for 30 min, 2.0 mL of hydrogen peroxide (30 wt %) was dropped in. Then the solution mixture was vigorously stirred for 20 min. Subsequently, the precursor solution was transferred to a Teflon-lined stainless steel autoclave (with a volume of 50.0 mL). The autoclave was maintained at 100 °C for 24 h and then heated to and maintained at 200 °C for 24 h. After cooling down to room temperature, a brown solution was obtained. The resultant SiO_2@Fe_3O_4@carbon NPs were then separated and washed with acetone several times. The as-prepared SiO_2@Fe_3O_4@carbon NP samples were then collected for further use.

Synthesis of HMMC-NCs

The as-prepared SiO_2@Fe_3O_4@carbon NPs (0.5 g) were redispersed in 30 mL ammonia water in order to remove the SiO_2 templates. After the solution was intensely sonicated for 30 min, the precursor solution was transferred to a Teflon-lined stainless steel autoclave (with a volume of 50.0 mL). The autoclave was heated to and maintained at 200 °C for 24 h. After cooling down to room temperature, the resultant HMMC-NCs were then separated and washed with distilled water several times. Finally, the HMMC-NCs were collected for further use.

Synthesis of chitosan-HMMC-NCs

Chitosan-HMMC-NCs were obtained by coupling the carboxyl group of HMMC-NCs and the amino group of chitosan molecules to form amide bonds. 5 mg EDC was added to 10 mL HMMC-NCs in PBS solution with a HMMC-NC concentration of 0.1 mg/mL. The solution was kept for 1 h at room temperature to activate carboxylate groups. The mixture was then added to 1 mL chitosan solution (5 mg/mL) with gentle stirring in darkness. The solution was reacted for 12 h, which resulted in the formation of amide bonds. Following this, the precipitates were centrifuged (14,000 rpm, 30 min) and washed with PBS buffer (5 mL) three times. Finally, chitosan-HMMC-NCs were collected for further use.

Synthesis of DOX-loaded HMMC-NCs and DOX-loaded chitosan-HMMC-NCs

Drug loading was performed by adding HMMC-NCs (1 mg) into 10 mL PBS solution (0.005 M, pH = 7.4) containing 2 mg DOX under magnetic stirring at 37 °C for 48 h. The mixture was then separated with an external magnetic field. In order to remove unloaded DOX adsorbed physically on the outer surface of the carbon shell of HMMC-NCs, the precipitate was redispersed in 10 mL PBS solution (pH = 7.4) and further purified by repeated separation and washing until the separated solution became clear. All the washed and separated solutions were collected and combined. The amount of unloaded free-DOX molecules in the combined solution was quantified by a UV-Vis spectrophotometer at 480 nm. The drug loading content of HMMC-NCs was calculated by $[(M_0 - M_t)/(M_N + M_0 - M_t)] \times 100\%$, where M_0 and M_t are the mass of DOX in the initial solution and separated solution, respectively and M_N is the mass of HMMC-NCs used in the loading process.

5 mg EDC was added to 10 mL of DOX-loaded chitosan-HMMC-NCs solution and allowed to react for 1 h at room temperature to activate carboxylate groups. The mixture was then

added to 1 mL chitosan solution (5 mg/mL) with gentle stirring in darkness. The solution was allowed to react for 12 h, which resulted in the formation of amide bonds. Following this, the solution was centrifuged (14,000 rpm, 30 min) to obtain precipitates that were washed with PBS buffer (5 mL) three times. All the washed and separated solutions were collected and combined. The amount of released DOX molecules in the combined solution was quantified by a UV-Vis spectrophotometer at 480 nm. Finally, the DOX-loaded chitosan-HMMC-NCs was collected for further use.

In vitro DOX release from DOX-loaded HMMC-NCs and DOX-loaded chitosan-HMMC-NCs

The *in vitro* release profiles of DOX from DOX-loaded HMMC-NCs and DOX-loaded chitosan-HMMC-NCs were acquired by the dialysis method. DOX-loaded HMMC-NCs and DOX-loaded chitosan-HMMC-NCs were redispersed in 10 mL PBS solution (0.005 M, pH = 7.4). The magnetic field-triggered release experiments of DOX-loaded HMMC-NCs and DOX-loaded chitosan-HMMC-NCs were performed at 37 °C by applying an AC magnetic field at various time intervals using a magnetic generator (110 V, 400 A). The released DOX molecules outside the dialysis bags were sampled at defined time periods and assayed by UV-Vis spectrometry at 480 nm. Cumulative release is expressed as the total percentage of drug released through the dialysis membrane over time.

Cell culture

Human glioblastoma cells, SF-763, were purchased from the American Type Culture Collection (ATCC) and grown in Dulbecco's Modified Eagle's Medium (DMEM) supplemented with 10% fetal bovine serum and 1% antibiotic-antimycotic (Life technologies, Grand Island, NY). Cells were cultured in an incubator maintained at 37 °C and 5% CO_2 with 95% humidity.

Laser confocal imaging of SF-763 cells treated with chitosan-HMMC-NCs

SF-763 cells were seeded onto glass cover slips in a 6-well plate. After overnight incubation in cell culture medium, cells were incubated with chitosan-HMMC-NCs (0.05 mg/mL) for 2 h. Cells were then washed with cold PBS 3× and fixed with 4% paraformaldehyde for 15 min at 37°C. Cells were then mounted onto glass slides with ProLong® Gold Antifade Mountant (Life Technologies Inc., Gaithersburg, MD). Images of cells were acquired using a Laser Scanning Microscope Leica SP8X (Leica Microsystems GmbH, Germany). Three excitation wavelengths were used: 405, 488 and 546 nm. The emission regions were 425–480 nm, 508–540 nm, and 566–700 nm, respectively.

Magnetic resonance imaging of chitosan-HMMC-NCs

The R_2 relaxivity ($1/T_2$) values of chitosan-HMMC-NCs in PBS at different concentrations were evaluated at 14 T using a multi-spin echo acquisition technique. Chitosan-HMMC-NCs in solution were pipetted into glass vials (3.25 mm I.D., 5 mm O.D., 200 μL volume). The vials were fastened together and placed into a water reservoir, which served as a homogeneous background signal to minimize magnetic susceptibility variations near the samples. The secured vials were placed in a 25 mm single-channel ^1H radiofrequency coil (PB Micro 2.5). Chitosan-HMMC-NCs were imaged with a quantitative T_2 multi-spin multi

echo scan sequence (MSME) (TR = 2,500 ms, TE = 6.7 + 6n ms, [n = 0–16], in-plane resolution 78 × 156 μm^2, matrix 256 × 128) with 0.5 mm thickness of each slice for 14 slices. Analysis of MRI data was accomplished with the FMRIB software library (FSL), Paravision 5.1 analysis package (Bruker), Osirix (Pixmeo) and ImageJ (NIH). T_2 values were determined within a circular, 100-voxel region of interest.

In vivo MRI

T_2-weighted imaging was performed on C57BL/6 wild-type mice prior to and after chitosan-HMMC-NC injection (100 μL, 0.5 mg/mL), using a Bruker Avance III 600 MHz, 14 T vertical-bore imaging system. Mice were anesthetized with isoflurane (Piramal Healthcare), and fixated in a coil-integrated respiratory monitoring system (SA Instruments; MR-compatible small animal monitoring and gating system) with nose-cone for oxygen/anesthetic, ear-bar head holder, circulating temperature control bath, respiratory monitoring, and residual gas extraction. Abdominal scans were acquired using rapid acquisition with refocused echoes (RARE) T_2-weighted (TR/TE = 691/5.5 ms, in-plane resolution 93 × 62 μm^2, matrix 256 × 284) sequences with slices placed in the transverse plane with 0.5 mm slice thickness and 0.75 mm interslice gap allowing for coverage from the liver to the pelvic floor.

Two-photon fluorescent imaging of SF-763 cells treated with chitosan-HMMC-NCs

SF-763 cells were seeded onto glass cover slips in a 24-well plate. Twenty four hours after seeding, cells were incubated with chitosan-HMMC-NCs (0.05 mg/mL) for 2 h. Cells were then washed with PBS 3× and fixed with 4% paraformaldehyde for 10 min. Nuclei were stained with DAPI before cells were mounted onto glass slides with ProLong® Gold Antifade Mountant (Life Technologies Inc., Gaithersburg, MD). Two-photon imaging was performed using an Olympus FV1000 MPE BX61 multi-photon microscope with excitation wavelength of 900 nm.

Viability of cells treated with drug-free and DOX-loaded HMMC-NCs or chitosan-HMMC-NCs with and without AC magnetic field irradiation

Cells were seeded in a 96-well plate and incubated overnight in the aforementioned growth conditions. On the following day, the medium was replaced with a medium containing drug-free or DOX-loaded HMMC-NCs/chitosan-HMMC-NCs or with a control medium. Three different sample concentrations (50, 25 and 12.5 mg/mL) were used, and samples at each concentration were ran in triplicate. The cells were incubated with drug-free or DOX-loaded HMMC-NCs/chitosan-HMMC-NCs for 72 h. Wells using the normal medium without drugs were used as the control. For magnetic-thermal treatments, the cells in the wells were irradiated with an AC magnetic field for 30 min. Cell viability was assessed using the alamar blue assay. Briefly, the medium was replaced with cell culture medium containing reagent and allowed to incubate for 2 h. Following the incubation, a microplate reader (SpectraMax i3, Molecular Devices, Sunnyvale, CA) was used to determine the fluorescence intensity of the dye (550ex/590em). The fluorescence intensities from drug-free and DOX-loaded HMMC-NCs/chitosan-HMMC-NCs treated cells were compared to that from untreated control cells to determine percent viability.

Histopathological Evaluation of DOX-loaded chitosan-HMMC-NCs and chitosan-HMMC-NCs

All animal experiments were conducted in accordance with University of Washington Institutional Animal Care and Use Committee approved protocols. Five days after intravenous administration of DOX-loaded chitosan-HMMC-NCs or chitosan-HMMC-NCs at 1 mg/mL, whole organs (heart, kidney, liver, lung and spleen) of C57BL/6 mice were removed through necropsy and preserved in 10% formalin for 48 h. Tissues were then embedded in paraffin, sliced into 5 μm sections, and stained with hematoxylin and eosin. Microscopic images of tissues were acquired using a Nikon ECLIPSE TE2000-S microscope.

Biodistribution of chitosan-HMMC-NCs

Mice were injected via tail vein with 200 μL of 1 mg/mL of Cy5.5-labelled chitosan-HMMC-NCs. Mice receiving no injection were used as controls. At 24, 48, and 72 h after injection, mice were euthanized and whole organs of liver, spleen, kidney, lung, and heart were harvested. Fluorescence was acquired for each organ using an Xenogen IVIS imaging system.

In vivo therapy of DOX-loaded chitosan-HMMC-NCs with/without AC magnetic field irradiation

Flank xenograft tumors of C6 cells were prepared by subcutaneous injection of one million cells suspended in serum free media and Matrigel (BD Biosciences, San Jose, CA) into NU/J mice (Jackson Labs, Bar Harbor, ME). Tumors were allowed to grow for 2 weeks before mice were injected intratumorally with nanocarrier samples. Mice were divided into four groups (n = 5 per group) injected with 200 μL of PBS, chitosan-HMMC-NCs, or DOX-loaded chitosan-HMMC-NCs (1 mg/mL, dose of DOX = 5.37 mg/kg). After 24 h, tumors were either subjected to or not subjected to the trement with an applied AC magnetic field for 30 min repeated every 3 d for a total of four times. Tumor volumes were assessedevery 2 days for 14 days. The length and width of the tumor were measured using a digital caliper. The tumor volume was calculated based on the following formula: $\text{width}^2 \times \text{length}/2$.

Characterization

TEM images were acquired on an FEI TECNAI transmission electron microscope at an accelerating voltage of 100 kV. High-resolution transmission electron microscopy images were acquired by JEM 2100 with an acceleration voltage of 200 kV. High-angle annular dark-field scanning transmission electron microscopy images were obtained using transmission electron microscopy (JEM-ARM200F) to characterize the nanostructure of the nanoparticles. UV-Vis absorption spectra were obtained on a Thermo Electron Co. Helios β UV-Vis Spectrometer. X-ray diffraction patterns were collected on a Japan Rigaku D/MAX-γA X-ray diffractometer over the 2θ range of 20–70°. Raman spectra were acquired on a LABRAM-HR Confocal Laser Micro-Raman spectrometer using an Ar^+ laser with 514.5 nm excitation at room temperature. FT-IR spectra were recorded with a Nicolet Instrument Co. MAGNA-IR 750 Fourier transform infrared spectrometer. The PL spectra were obtained on a JOBIN YVON Co. FluoroMax®-3 Spectrofluorometer equipped with a Hamamatsu

R928P photomultiplier tube, calibrated photodiode for excitation reference correction from 200 to 980 nm and an integration time of 1 second. The hydrodynamic size and surface charge of nanocarriers were determined using a Zetasizer Nano-ZS (Malvern Instruments, Worcestershire, UK) at room temperature. A superconducting quantum interference device (SQUID) magnetometer (Quantum Design MPMS XL-7) was used to measure the magnetic properties of the NPs. Nitrogen adsorption–desorption measurements were carried out on a Micromeritics ASAP 2010 instrument to determine the BET surface area, single point total pore volume and pore size distribution.

Supplementary Material

Refer to Web version on PubMed Central for supplementary material.

Acknowledgments

We gratefully acknowledge the financial support from NIH grant (R01CA161953), Kyocera professor endowment, and American Diabetes Association (Basic Science Award 1-12-BS-243). The two photon fluorescence imaging study was supported in part by a gift to the Institute for Stem Cell and Regenerative Medicine at the University of Washington. P.J.P. gratefully acknowledges support from both the US Department of Energy's Pacific Northwest National Laboratory (PNNL) and the Materials Synthesis and Simulation Across Scales (MS3) Initiative, a Laboratory Directed Research and Development (LDRD) program at the PNNL. The PNNL is operated by Battelle under Contract DEAC05-76RL01830.

References

1. Wang AZ, Langer R, Farokhzad OC. Annu Rev Med. 2012; 63:185. [PubMed: 21888516]
2. Mura S, Nicolas J, Couvreur P. Nat Mater. 2013; 12:991. [PubMed: 24150417]
3. Kievit FM, Zhang M. Adv Mater. 2011; 23:H217. [PubMed: 21842473]
4. Ganta S, Devalapally H, Shahiwala A, Amiji M. J Control Release. 2008; 126:187. [PubMed: 18261822]
5. Horcajada P, Chalati T, Serre C, Gillet B, Sebrie C, Baati T, Eubank JF, Heurtaux D, Clayette P, Kreuz C, Chang JS, Hwang YK, Marsaud V, Bories PN, Cynober L, Gil S, Ferey G, Couvreur P, Gref R. Nat Mater. 2010; 9:172. [PubMed: 20010827]
6. Liu R, Zhao X, Wu T, Feng P. J Am Chem Soc. 2008; 130:14418. [PubMed: 18841893]
7. Descalzo AB, Martínez-Máñez R, Sancenón F, Hoffmann K, Rurack K. Angew Chem Int Ed. 2006; 45:5924.
8. Saha S, Leung KCF, Nguyen TD, Stoddart JF, Zink JI. Adv Funct Mater. 2007; 17:685.
9. Slowing II, Vivero-Escoto JL, Wu CW, Lin VSY. Adv Drug Del Rev. 2008; 60:1278.
10. Wu S, Huang X, Du X. Angew Chem Int Ed. 2013; 52:5580.
11. Lai CY, Trewyn BG, Jeftinija DM, Jeftinija K, Xu S, Jeftinija S, Lin VSY. J Am Chem Soc. 2003; 125:4451. [PubMed: 12683815]
12. Nguyen TD, Liu Y, Saha S, Leung KCF, Stoddart JF, Zink JI. J Am Chem Soc. 2007; 129:626. [PubMed: 17227026]
13. Liu R, Zhang Y, Feng P. J Am Chem Soc. 2009; 131:15128. [PubMed: 19746981]
14. Aznar E, Marcos MD, Martínez-Máñez R, Sancenón F, Soto J, Amorós P, Guillem C. J Am Chem Soc. 2009; 131:6833. [PubMed: 19402643]
15. Vivero-Escoto JL, Slowing II, Wu CW, Lin VSY. J Am Chem Soc. 2009; 131:3462. [PubMed: 19275256]
16. Ruiz-Hernández E, Baeza A, Vallet-Regí M. ACS Nano. 2011; 5:1259. [PubMed: 21250653]
17. Li Z, Zhang Y, Wu X, Wu X, Maudgal R, Zhang H, Han G. Adv Sci. 2015; 2:1500001.
18. Goel S, Chen F, Luan S, Valdovinos HF, Shi S, Graves SA, Ai F, Barnhart TE, Theuer CP, Cai W. Adv Sci. 2016; 3:1600122.

19. Huo M, Chen Y, Shi J. Expert Opin Drug Del. 2016; 13:1195.
20. Chen Y, Chen H, Shi J. Adv Mater. 2013; 25:3144. [PubMed: 23681931]
21. Chen Y, Shi J. Adv Mater. 2016; 28:3235. [PubMed: 26936391]
22. Tang F, Li L, Chen D. Adv Mater. 2012; 24:1504. [PubMed: 22378538]
23. Zhou S, Du X, Cui F, Zhang X. Small. 2014; 10:980. [PubMed: 24745059]
24. Acosta C, Pérez-Esteve E, Fuenmayor CA, Benedetti S, Cosio MS, Soto J, Sancenón F, Mannino S, Barat J, Marcos MD, Martínez-Máñez R. ACS Appl Mater Interfaces. 2014; 6:6453. [PubMed: 24707920]
25. Yang X, Liu X, Liu Z, Pu F, Ren J, Qu X. Adv Mater. 2012; 24:2890. [PubMed: 22539076]
26. Chang YT, Liao PY, Sheu HS, Tseng YJ, Cheng FY, Yeh CS. Adv Mater. 2012; 24:3309. [PubMed: 22648937]
27. Casasús R, Climent E, Marcos MD, Martínez-Máñez R, Sancenón F, Soto J, Amorós P, Cano J, Ruiz E. J Am Chem Soc. 2008; 130:1903. [PubMed: 18211068]
28. Wang X, Cai X, Hu J, Shao N, Wang F, Zhang Q, Xiao J, Cheng Y. J Am Chem Soc. 2013; 135:9805. [PubMed: 23789713]
29. Zhu CL, Lu CH, Song XY, Yang HH, Wang XR. J Am Chem Soc. 2011; 133:1278. [PubMed: 21214180]
30. Li N, Yu Z, Pan W, Han Y, Zhang T, Tang B. Adv Funct Mater. 2013; 23:2255.
31. Yu Z, Li N, Zheng P, Pan W, Tang B. Chem Commun. 2014; 50:3494.
32. Lee SM, Park H, Yoo KH. Adv Mater. 2010; 22:4049. [PubMed: 20665571]
33. Chen MC, Ling MH, Wang KW, Lin ZW, Lai BH, Chen DH. Biomacromolecules. 2015; 16:1598. [PubMed: 25839774]
34. Licciardi M, Scialabba C, Fiorica C, Cavallaro G, Cassata G, Giammona G. Mol Pharm. 2013; 10:4397. [PubMed: 24168360]
35. Mo R, Jiang T, DiSanto R, Tai W, Gu Z. Nat Commun. 2014; 5:3364. [PubMed: 24618921]
36. Pernia Leal M, Torti A, Riedinger A, La Fleur R, Petti D, Cingolani R, Bertacco R, Pellegrino T. ACS Nano. 2012; 6:10535. [PubMed: 23116285]
37. Wang H, Di J, Sun Y, Fu J, Wei Z, Matsui H, del C Alonso A, Zhou S. Adv Funct Mater. 2015; 25:5537.
38. Wang H, Cao G, Gai Z, Hong K, Banerjee P, Zhou S. Nanoscale. 2015; 7:7885. [PubMed: 25854197]
39. Guisasola E, Baeza A, Talelli M, Arcos D, Moros M, de la Fuente JM, Vallet-Regí M. Langmuir. 2015; 31:12777. [PubMed: 26536300]
40. Liu TY, Liu KH, Liu DM, Chen SY, Chen IW. Adv Funct Mater. 2009; 19:616.
41. Di Corato R, Espinosa A, Lartigue L, Tharaud M, Chat S, Pellegrino T, Ménager C, Gazeau F, Wilhelm C. Biomaterials. 2014; 35:6400. [PubMed: 24816363]
42. Hayashi K, Nakamura M, Miki H, Ozaki S, Abe M, Matsumoto T, Sakamoto W, Yogo T, Ishimura K. Theranostics. 2014; 4:834. [PubMed: 24955144]
43. Brazel CS. Pharm Res. 2009; 26:644. [PubMed: 19005741]
44. Wang H, Wei Z, Matsui H, Zhou S. J Mater Mater A. 2014; 2:15740.
45. Lee D, Gemici Z, Rubner M, Cohen R. Langmuir. 2007; 23:8833. [PubMed: 17628090]
46. Wang H, Shen J, Li Y, Wei Z, Cao G, Gai Z, Hong K, Banerjee P, Zhou S. Biomater Sci. 2014; 2:915.
47. Ge J, Hu Y, Biasini M, Beyermann WP, Yin Y. Angew Chem Int Ed. 2007; 46:4342.
48. Ferrari AC, Robertson J. Phys Rev B. 2000; 61:14095.
49. Ristein J, Stief RT, Ley L, Beyer W. J Appl Phys. 1998; 84:3836.
50. Chang YR, Lee HY, Chen K, Chang CC, Tsai DS, Fu CC, Lim TS, Tzeng YK, Fang CY, Han CC, Chang HC, Fann W. Nat Nanotechnol. 2008; 3:284. [PubMed: 18654525]
51. Cao L, Wang X, Meziani MJ, Lu F, Wang H, Luo PG, Lin Y, Harruff BA, Veca LM, Murray D, Xie SY, Sun YP. J Am Chem Soc. 2007; 129:11318. [PubMed: 17722926]
52. Denk W, Strickler J, Webb W. Science. 1990; 248:73. [PubMed: 2321027]

53. Helmchen F, Denk W. Nat Meth. 2005; 2:932.
54. Sun X, Liu Z, Welsher K, Robinson JT, Goodwin A, Zaric S, Dai H. Nano Res. 2008; 1:203. [PubMed: 20216934]
55. Ma M, Chen H, Chen Y, Wang X, Chen F, Cui X, Shi J. Biomaterials. 2012; 33:989. [PubMed: 22027594]
56. Wang H, Sun Y, Yi J, Fu J, Di J, del Carmen Alonso A, Zhou S. Biomaterials. 2015; 53:117. [PubMed: 25890712]
57. Hahn GM, Braun J, Har-Kedar I. Proc Natl Acad Sci U S A. 1975; 72:937. [PubMed: 48253]
58. Wang H, Wang K, Tian B, Richard R, Mu Q, Jeon M, Chang F, Zhang M. Small. 2016; doi: 10.1002/smll.201602263

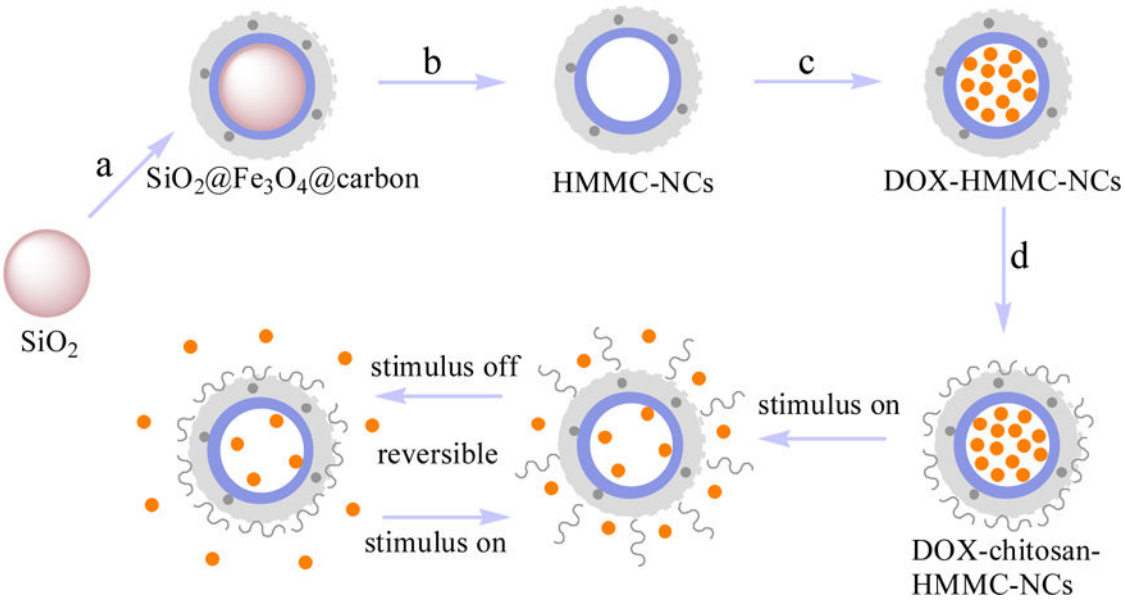

Figure 1.

Schematic design of magnetic field-triggered on/off drug release system. Black dots in the carbon shell (light grey) represent carbon quantum dots. The pink sphere represents SiO2 nanoparticle core as templete. Orange dots represent DOX molecules. Black chains represent chitosan valves. (a) Surface coating of SiO_2 core. (b) Erosion of the SiO_2 core and formation of HMMC-NCs. (c) Loading of DOX into HMMC-NCs. (d) Surface modification of DOX-HMMC-NCs with chitosan molecules to form DOX-chitosan-HMMC-NCs.

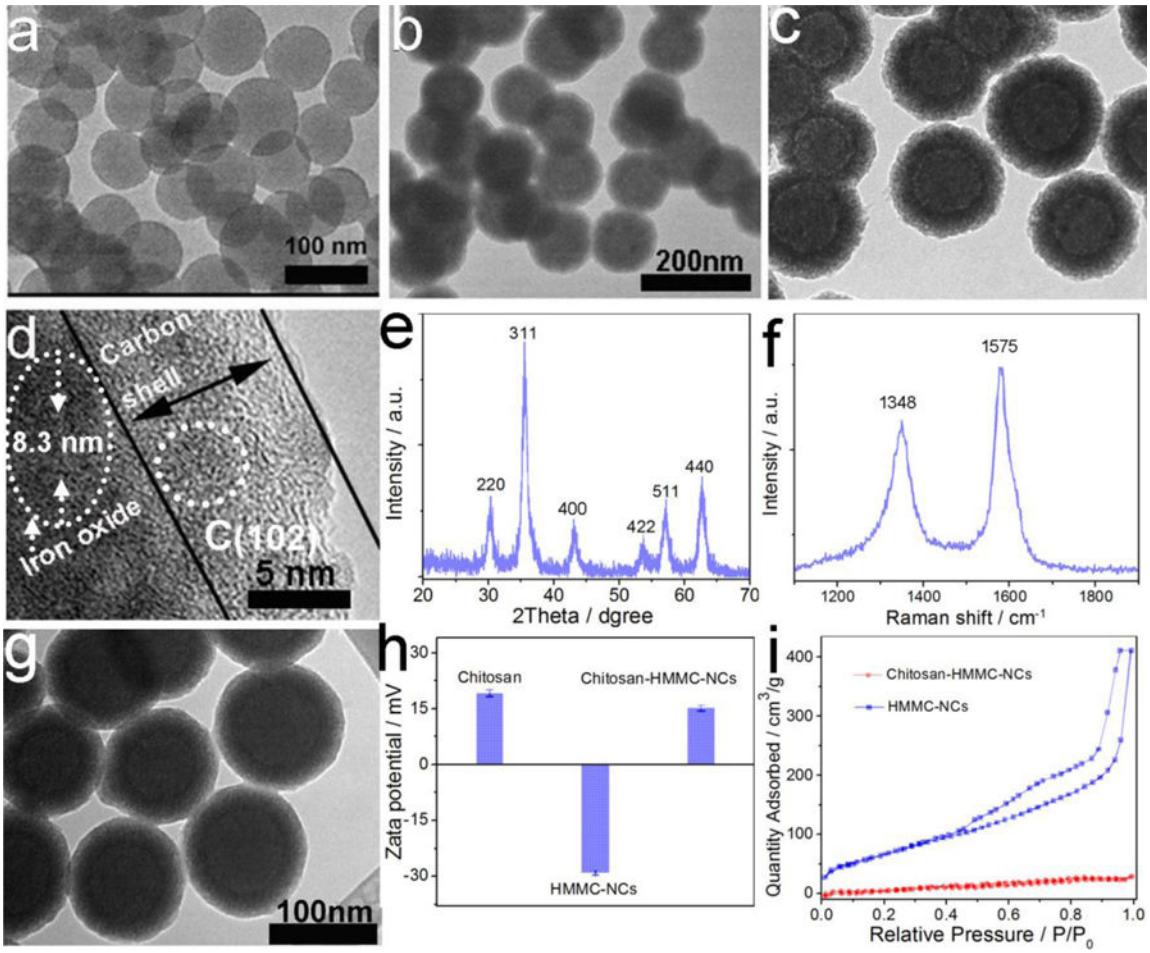

Figure 2.

Morphology and phase characterization of HMMC-NCs and chitosan-HMMC-NCs. (a and b) Representative TEM images of SiO_2 cores as template and SiO_2@Fe_3O_4@carbon NPs, respectively. (c) TEM image of HMMC-NCs. (d) High resolution TEM image of a dual-layer shell of a HMMC-NC. (e and f) XRD pattern and Raman spectrum, respectively, of as-obtained HMMC-NCs. (g) TEM image of chitosan-HMMC-NCs. (h) zeta potential of chitosan, HMMC-NC and chitosan-HMMC-NCs. (i) N_2 adsorption-desorption isotherms of HMMC-NCs and chitosan-HMMC-NCs.

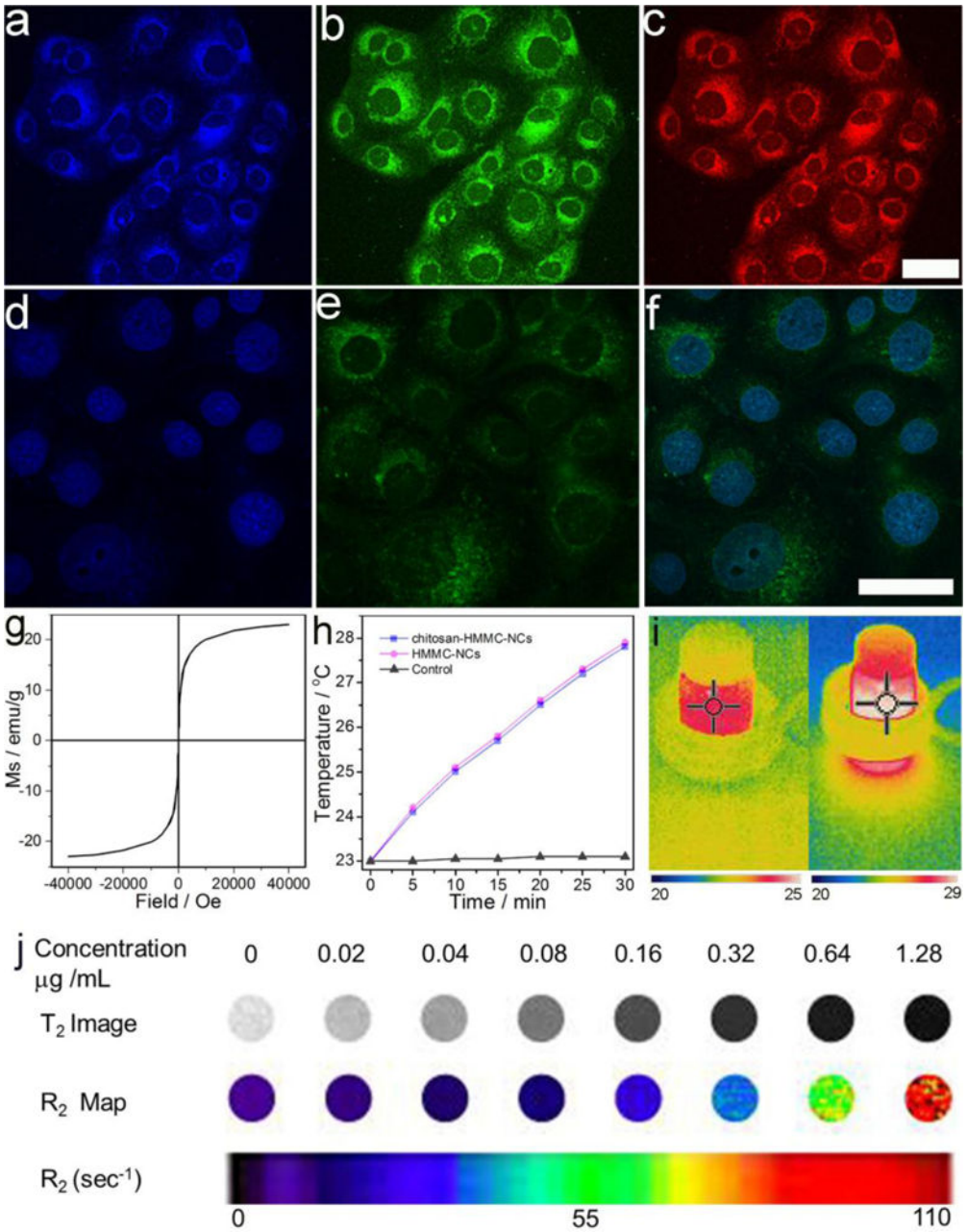

Figure 3.

Dual-modal optical imaging and magnetic property of chitosan-HMMC-NCs. Laser scanning confocal microscopic images of SF-763 cells incubated with chitosan-HMMC-NCs for 2 h and irradiated with laser under different excitation wavelengths: (a) 405 nm, (b) 488 nm, and (c) 546 nm. (d) DAPI nuclear stain. (e) Two-photon fluorescence. (f) Overlaid DAPI and fluorescence images of SF-763 cells incubated with chitosan-HMMC-NCs under the laser excitation of the wavelength of 900 nm. Scale bars = 50 μm. (g) Magnetization curve of chitosan-HMMC-NCs measured at room temperature. (h) The temperature curves of water, HMMC-NCs (0.1 mg/mL) and chitosan-HMMC-NCs (0.1 mg/mL) under an AC magnetic field for 30 min. (i) IR thermal images of chitosan-HMMC-NCs (0.1 mg/mL) in

water under an AC magnetic field with different treatment times: 0 min (left) and 30 min (right). (j) R_2 maps of MRI phantoms of chitosan-HMMC-NCs taken at different concentrations.

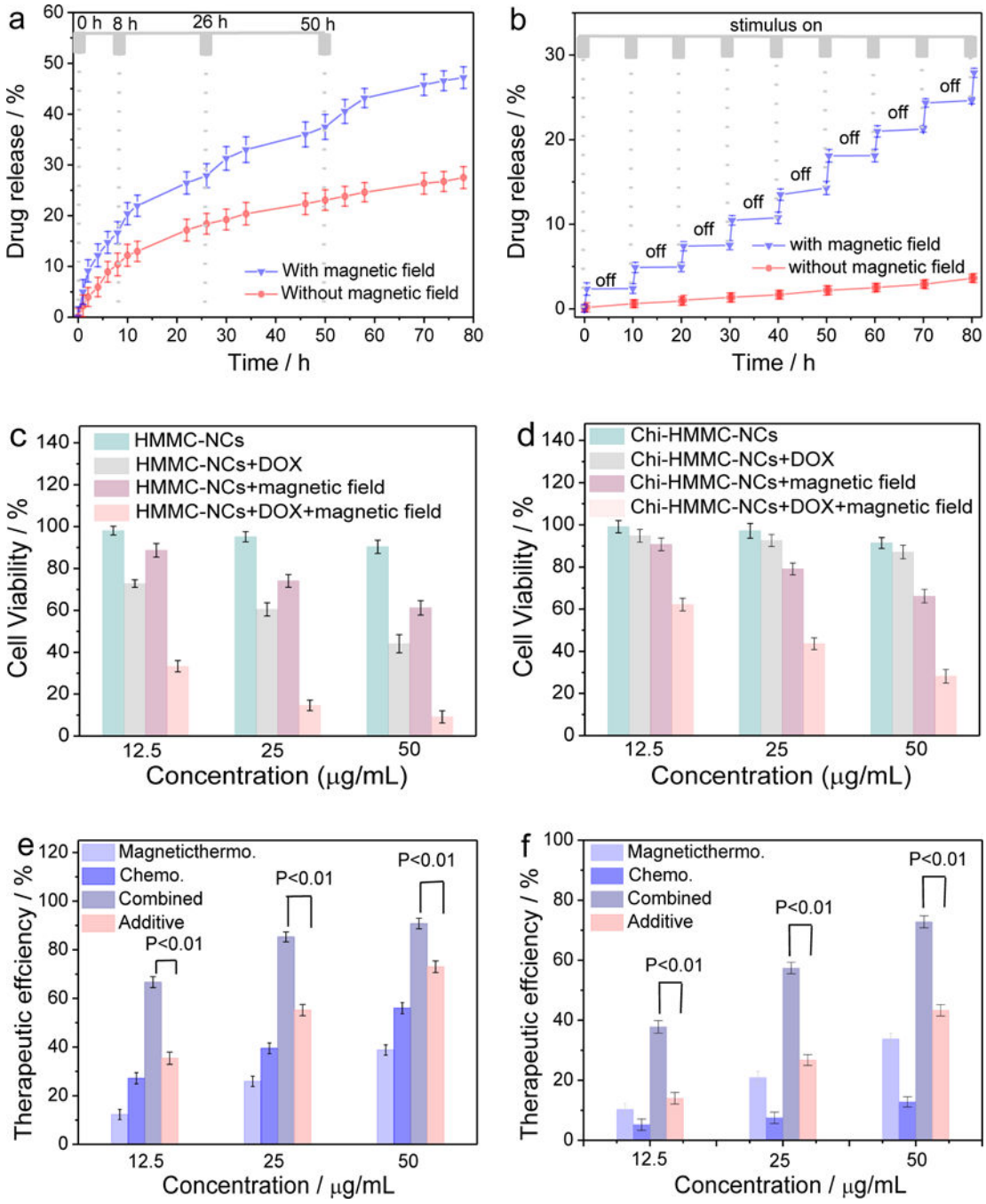

Figure 4.

Drug release and *in vitro* cytotoxicity studies. DOX release profiles of (a) HMMC-NCs and (b) chitosan-HMMC-NCs in PBS at 37°C, induced with/without irradiation of an external AC magnetic field for 30 min at various time points of drug release process. (c) *In vitro* cytotoxicity induced by drug-free HMMC-NCs and DOX-loaded HMMC-NCs without and with irradiation of an external AC magnetic field for 30 min. (d) *In vitro* cytotoxicity of drug-free chitosan-HMMC-NCs and DOX-loaded chitosan-HMMC-NCs with/without irradiation of an external AC magnetic field for 30 minutes. Therapeutic efficiencies of (e)

HMMC-NCs and (f) chitosan-HMMC-NCs as DOX carriers and magnetic-thermal therapy agents for chemo, magnetic-thermal, and combined (synergistic) treatments. Also included is the result of additive combination of chemo and magnetic-thermal treatment, evaluated by simple weighted addition of chemo and magnetic-thermal treatments.

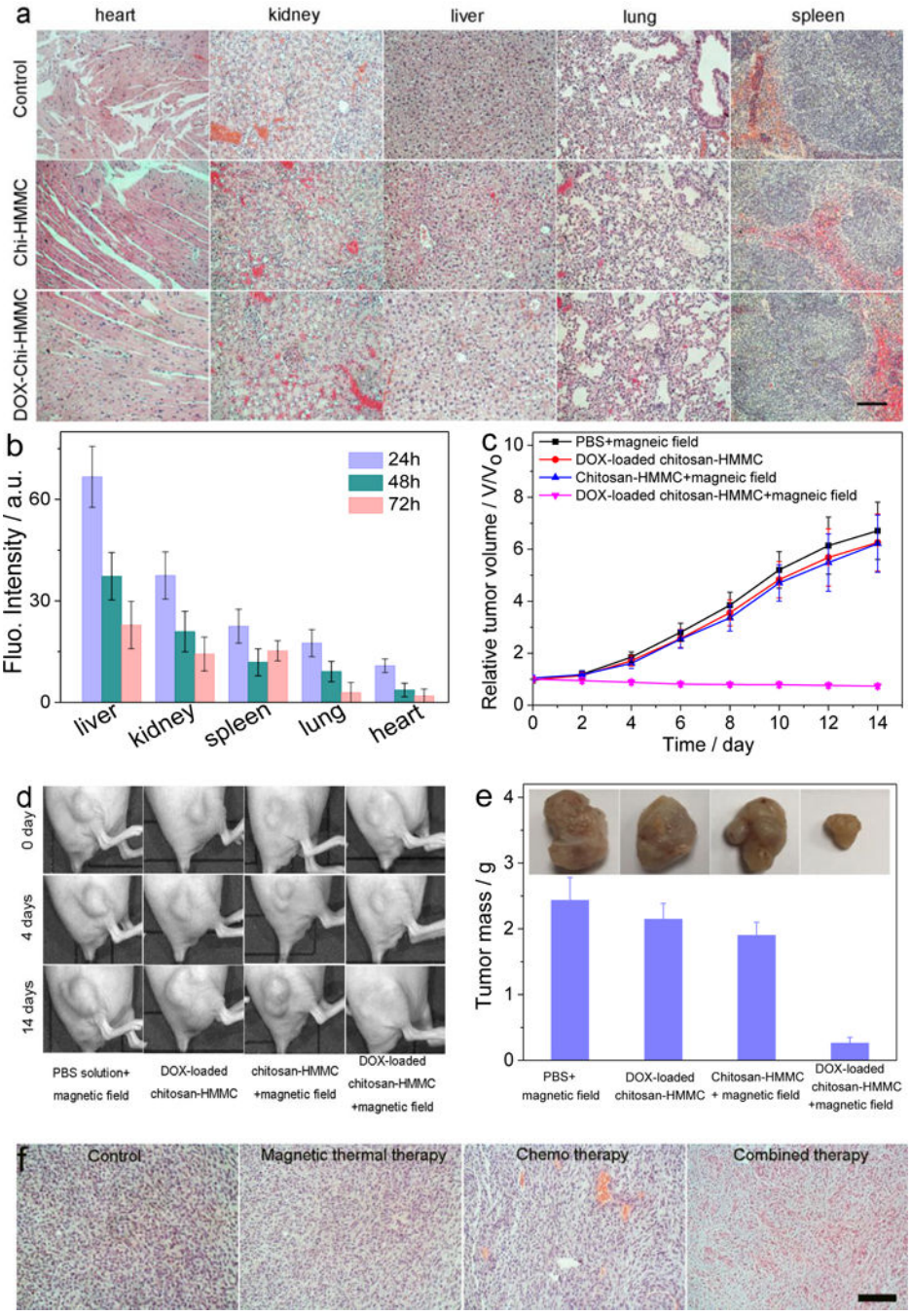

Figure 5.

In vivo toxocity and therapy of chitosan-HMMC-NCs and DOX-loaded chitosan-HMMC-NCs. (a) H&E stained tissue sections of mouse heart, kidney, liver, lung and spleen obtained from noninjected mice, those injected with chitosan-HMMC-NCs or DOX-loaded chitosan-HMMC-NCs at a concentration of 1 mg mL^{-1}. The scale bar = 125 μm. (b) Biodistributions of chitosan-HMMC-NCs in different organs of nude mice determined at 24 h post-injection. (c) The tumor volume growth curves of mice after various treatments (intratumoral injection, four mice for each group). Error bars were based on standard error of the mean (SEM). (d)

Photographs of tumors in mice under various treatments at different treatments days. (e) Average weights and photographs (inset) of tumors collected from mice at the end of treatments (day 14). (f) H&E-stained tumor sections collected from mice post treatments (scale bar = 125 μm).